Atom Probe Tomography of *a*-Axis GaN Nanowires: Analysis of Nonstoichiometric Evaporation Behavior

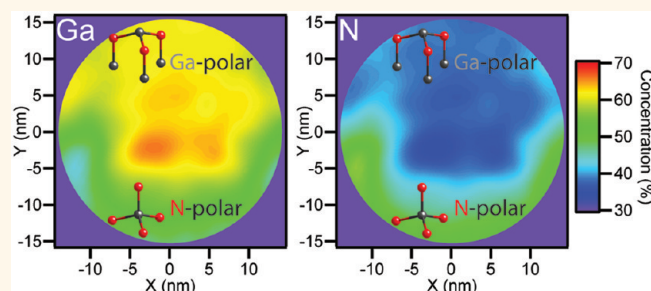**James R. Riley,[†] Rodrigo A. Bernal,[‡] Qiming Li,[§] Horacio D. Espinosa,[‡] George T. Wang,[§] and Lincoln J. Lauhon[†,*]**

[†]Department of Materials Science and Engineering, Northwestern University, Evanston, Illinois 60208, United States, [‡]Department of Mechanical Engineering, Northwestern University, Evanston, Illinois 60208, United States, and [§]Sandia National Laboratories, Albuquerque, New Mexico 87185, United States

Group III—Nitride alloys are direct wide-band-gap semiconductors that emit light from the ultraviolet into the visible spectrum, making them a useful foundation for light-emitting devices.[1] In the wurtzite structure, GaN—InGaN heterostructures that are grown normal to the polar *c*-plane possess internal electric fields as large as ~1 MV/cm.[2] This causes a spatial separation of electron and hole wave functions within InGaN quantum wells (QWs), reducing the carrier radiative recombination rate and internal quantum efficiency (IQE).[3,4] Such effects can be avoided by growing along nonpolar orientations, such as the *a*-axis, but *a*-axis GaN films exhibit high stacking fault and dislocation densities on common substrates such as sapphire or silicon, resulting from large lattice mismatches. These defects can act as nonradiative recombination centers that degrade IQE.[4—7] In contrast to thin films, *a*-axis nanowires can be grown virtually free of dislocations due to the small substrate interfacial area and termination of dislocations at the nanowire surface.[8,9] In addition, a core—shell nanowire geometry allows for high light extraction due to the large junction area and increased directionality of light emission.[9—11]

The development and optimization of light-emitting devices based on III—N nanostructures requires methods of characterizing dopant distribution and buried interfaces that are appropriate to nanoscale heterostructures. Atom probe tomography (APT) has a unique role in this regard, as it can analyze the composition of a solid with single-atom sensitivity and subnanometer spatial resolution in three dimensions.[12] Furthermore, the commercialization of pulsed laser APT has facilitated the analysis of

semiconducting materials that could not be analyzed by voltage pulsing.[13] In pulsed laser APT, laser-assisted field evaporation is used to selectively remove ions at the tip of a nanoscale specimen; the positions and times of flight of ions registered by a 2-D detector are then used to create a 3-D reconstruction of the evaporated material. Pulsed laser APT has been used to map dopant distributions in single-element group IV nanowires,[14—16] but compound semiconductors

ABSTRACT

GaN nanowires oriented along the nonpolar *a*-axis were analyzed using pulsed laser atom probe tomography (APT). Stoichiometric mass spectra were achieved by optimizing the temperature, applied dc voltage, and laser pulse energy. Local variations in the measured stoichiometry were observed and correlated with facet polarity using scanning electron microscopy. Fewer N atoms were detected from nonpolar and Ga-polar surfaces due to uncorrelated evaporation of N_2 ions following N adatom diffusion. The observed differences in Ga and N ion evaporation behaviors are considered in detail to understand the influence of intrinsic materials characteristics on the reliability of atom probe tomography analysis. We find that while reliable analysis of III—N alloys is possible, the standard APT procedure of empirically adjusting analysis conditions to obtain stoichiometric detection of Ga and N is not necessarily the best approach for this materials system.

KEYWORDS: atom probe tomography · semiconductor nanowires · GaN

present an additional challenge because the constituent elements may exhibit dramatically different evaporation behaviors.

As early as the 1980s researchers made a concerted effort to understand the mechanisms that governed the evaporation of compound semiconductors during APT analysis. Due to differences in the evaporation fields of the group III and group V species, one type of atom was often detected more readily than the other, leading to inaccurate stoichiometries.[17−20] In addition, group V elements were observed to evaporate as clusters (e.g., As_2^+, As_3^+, As_4^+) in GaP,[21] GaInP,[22] GaAs,[22] GaInAs,[23,24] AlInAs,[24] and GaAlInAs.[24] Because the evaporation field for the group V species is higher in these cases, it was concluded that the atoms migrate over short distances on the surface to form clusters with evaporation fields comparable to the group III atoms.[23] Recent analyses of GaAs/GaInP/GaAs heterostructures reported observation of group V clustering, indicating that this phenomenon is prevalent even with state-of-the-art APT analyses.[25] Confronted with such complexities, one simple approach to reliable analysis is to optimize experimental conditions to achieve a known stoichiometry calibrated by some other technique, such as secondary ion mass spectroscopy. Such an approach is not possible with nanowire heterostructures. Furthermore, total stoichiometry optimization can actually lead to less reliable analysis, as we demonstrate below.

While the evaporation mechanisms of GaAs, GaP, and associated alloys have been comprehensively studied, GaN has received comparatively little attention. It is especially challenging to perform APT of GaN because of its low electrical conductivity; a pulsed laser is required to achieve reliable evaporation, and the mass resolution is degraded by the poor thermal conductivity.[26] In spite of these challenges, APT has been used to analyze dopant clustering and map interface uniformity in planar InGaN QWs,[6,27] GaN—AlGaN superlattice structures,[28] and c-axis GaN nanowires.[29] The latter study, using a 532 nm pulsed laser, reported variations in the evaporation behavior of Ga and N ions that was attributed to nonuniform heating at the nanowire tip. This heating led to a reduced detection of N due to evaporation that was not correlated with the laser pulses. This study reports empirical identification of experimental conditions that yield stoichiometric evaporation in APT.[29]

Here we report pulsed UV laser (355 nm) APT analysis of a-axis-oriented GaN nanowires that do not present artifacts caused by nonuniform heating. However, variations in surface curvature and faceting are found to strongly influence the measured stoichiometry. Specifically, the optimization of run conditions to achieve global stoichiometry results in a Ga deficiency on N-polar facets and a N deficiency on nonpolar and Ga-polar facets. The observations suggest that quantitative analysis of group III composition variations in III—N ternary alloys is possible, but that experimental conditions should be tailored to maximize the

signal-to-noise ratio rather than the stoichiometry. Such an approach is particularly important for the analysis of dilute impurities and dopants, both for nanowires and for specimens prepared from thin film heterostructures.

RESULTS AND DISCUSSION

GaN nanowires were mounted on tungsten microtips for analysis using APT, as depicted in Figure 1 and further discussed in the Materials and Methods section. Stoichiometric evaporation of Mg-doped nanowires was achieved by adjusting temperature, applied dc voltage, and pulse energy during the experiment. Peaks associated with Ga and N are readily resolved in the representative mass spectrum shown in Figure 1c. The N species evaporated predominantly as singly and doubly charged N_2 at 28 and 14 amu, respectively. While the 14 amu peak could contain both N^+ and N_2^{2+}, the similarities of the Ga^{2+}/Ga^+ and N_2^{2+}/N^+ charge state ratios suggest that N^+ does not make a significant contribution. Furthermore, no isotope peak $^{15}N^+$ was detected.[30] The nanowires were doped with Mg to increase the conductivity, which facilitates APT analysis, and to measure the dopant incorporation rate, which is not known for GaN nanowires. On the basis of the flow rates described in the Materials and Methods section, the Mg/Ga ratio in the gas phase during growth was 0.003. However, no Mg peaks were identified in the mass spectrum, indicating a relatively low doping efficiency for these growth conditions. The background noise level was used to establish a maximum Mg concentration of 140 ppm ($\sim 2 \times 10^{19}$ cm^{-3}) for the mass spectrum shown in Figure 1c. The mass spectrum with the highest signal-to-noise ratio, taken from a different nanowire, did not contain any Mg peaks and yielded an upper bound on the Mg concentration of 0.3 ppm ($\sim 5 \times 10^{16}$ cm^{-3}) assuming no preferential loss of Mg.

Previous scanning electron microscopy (SEM) and transmission electron microscope (TEM) imaging has shown that GaN nanowires grown epitaxially on r-plane sapphire using metal—organic chemical vapor deposition (MOCVD) typically grow vertically along the nonpolar [11$\bar{2}$0] direction (a-axis). Some a-axis nanowires grow 30° from vertical, and a small number of nanowires grow at 60° in the nonpolar [10$\bar{1}$0] direction (m-axis).[31,32] SEM imaging of the growth substrate for the nanowires used in this study revealed that 75% of the Mg-doped nanowires grew along an a-axis. As discussed in the Materials and Methods section, nanowires with suitable dimensions were selected and mounted on tungsten microtips. While the mounting process did not intentionally exclude m-axis nanowires, less than 7% of the observed m-axis nanowires were long enough (~ 8 μm) to mount. It is therefore unlikely that any m-axis nanowires were selected for investigation, and the discussion below assumes an a-axis orientation.
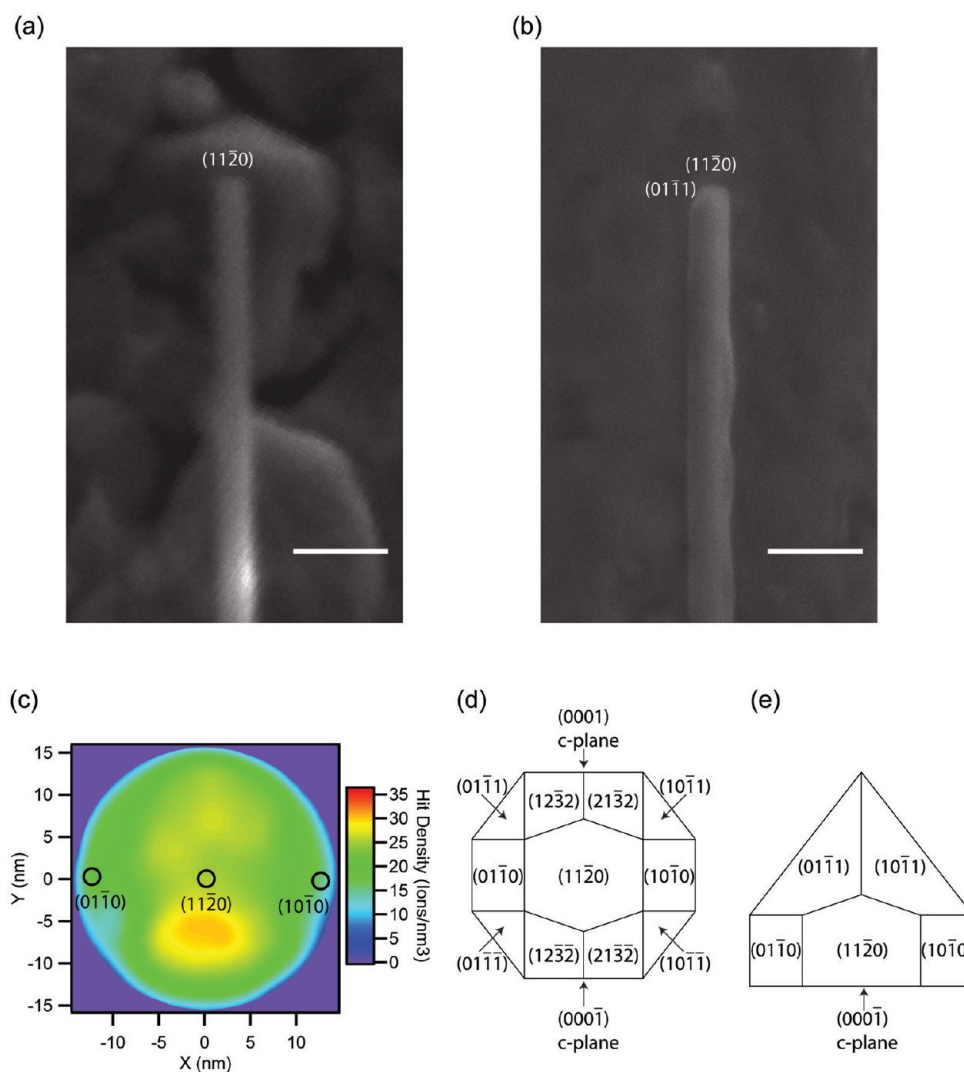
Anisotropic faceting of the nanowires, which develops during synthesis and evolves during APT analysis, was observed by SEM imaging and analysis of APT 2-D
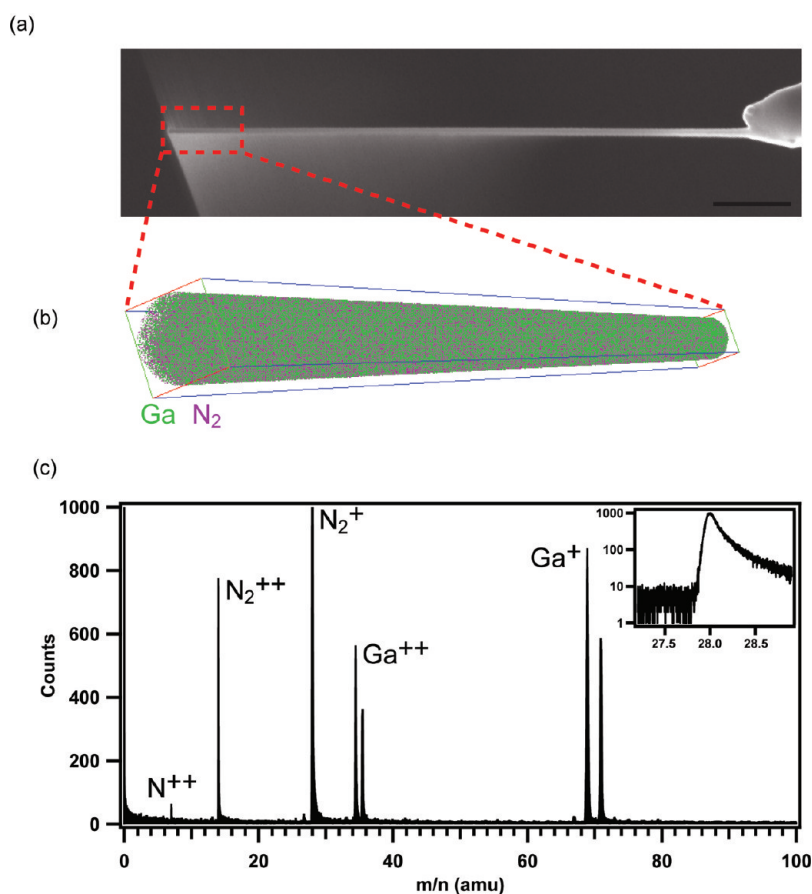
Figure 1. (a) SEM image of a GaN nanowire mounted on a W microtip. Scale bar is 1 μm. (b) Perspective view of a 3-D reconstruction of the nanowire with 20% of Ga and N_2 atoms displayed ($45 \times 45 \times 1016$ nm^3). (c) APT mass spectrum. The total amounts of Ga and N atoms were detected in nearly the correct stoichiometric ratio (N/Ga = 1.03). Inset: Semilog plot of N_2^+ peak showing thermally broadened tail.

hit density profiles. a-axis GaN nanowires exhibit isosceles triangular cross sections with two semipolar $\{\bar{1}101\}$ side facets of equivalent edge length and one polar c-plane side facet with ~7% shorter edge length.[33] Consistent with prior results, post-APT SEM imaging of one of the nanowires measured triangular side facet lengths (viewed from above) of 120 ± 3, 117 ± 5, and 110 ± 3 nm, corresponding to the $(1\bar{1}01)$, $(\bar{1}101)$, and $(000\bar{1})$ side facets of the nanowire. Negligible InGaN grows on the N-polar c-plane facet during synthesis of GaN/InGaN core/shell nanowires, indicating that the exposed c-plane is the N-polar $(000\bar{1})$ plane.[34−37] Qian et al. previously observed a similar lack of InGaN growth on triangular GaN nanowires with the same facet geometry as reported here and reported an N-polar $(000\bar{1})$ c-plane facet based on convergent-beam electron diffraction studies.[35] The $(000\bar{1})$ c-plane polarity was confirmed experimentally by wet etching of the nanowires in a KOH-based solution, resulting in the formation of nanotip pyramids on the c-plane facet (Supporting Information Figure S1). This selective wet etch is known to etch and cause the formation of nanotip pyramids for N-polar c-plane GaN and does not etch the Ga-polar c-plane surface.[38]

Pre- and post-APT SEM imaging shows that the end of the nanowire evolves from a single top plane to a multiply faceted surface (Figure 2a,b). The faceted tip morphology produces variations in the electric field at the evaporation surface that affect the trajectories of evaporated ions. The field variations are manifest as corresponding spatial variations in the density of ions hitting the detector, with a lower ion density associated with regions of higher local field divergence. Low-index planes often manifest as a region of lower hit density because the trajectories of ions evaporating from the terrace edges diverge more strongly as the size of the topmost terrace decreases during evaporation.[39−42] The 2-D hit density profile in Figure 2c was produced by plotting the number of ions detected as a function of lateral position for the entire reconstructed volume. The hit density profile exhibits a mirror plane at $x = 0$ ($y-z$ plane) but is not symmetric with respect to reflection about $y = 0$ ($x-z$ plane), as the c-axis of the polar crystal lacks inversion symmetry. Ten nanowires were analyzed by APT, and all showed the same symmetries in the 2-D hit density profile, enabling their azimuthal orientations to be determined unambiguously. Four examples are shown in Supporting Information Figure S2.

(a)

(b)

$(11\bar{2}0)$

$(11\bar{2}0)$
$(01\bar{1}1)$

(c)

(d)

(0001)
c-plane

$(01\bar{1}1)$ $(12\bar{3}2)$ $(21\bar{3}2)$ $(10\bar{1}1)$

$(01\bar{1}0)$ $(11\bar{2}0)$ $(10\bar{1}0)$

$(01\bar{1}\bar{1})$ $(12\bar{3}\bar{2})$ $(21\bar{3}\bar{2})$ $(10\bar{1}\bar{1})$

$(000\bar{1})$
c-plane

(e)

$(01\bar{1}1)$ $(10\bar{1}1)$

$(01\bar{1}0)$ $(11\bar{2}0)$ $(10\bar{1}0)$

$(000\bar{1})$
c-plane

Figure 2. SEM image of a GaN nanowire (a) before and (b) after APT analysis. Scale bar: 200 nm. (c) 2-D hit density profile depicting the total number of Ga+N atoms/nm³ detected for the entire reconstructed volume. The locations of the $(01\bar{1}0)$, $(11\bar{2}0)$, and $(10\bar{1}0)$ poles are indicated, assuming a vertical a-axis nanowire. (d) Schematic of selected low-index facets of GaN. (e) Facets present during selected area epitaxy reflecting facet stability.

The crystal orientation is shown in Figure 2d, together with several low-index facets that would be present to varying degrees during APT analysis in the absence of the c-axis anisotropy. For reference, the projections of the $(01\bar{1}0)$, $(11\bar{2}0)$, and $(10\bar{1}0)$ poles onto the 2-D hit density profile are shown in Figure 2c, assuming a vertical a-axis nanowire. The pole locations were determined using the equations governing the projection of a specimen tip onto the detector during APT.[39] Due to the similarities in the symmetries of the a- and m-axes, either orientation would exhibit poles within the field of view of the detector. However, the assigned poles for the a-axis orientation are of lower index and therefore in better agreement because low-index pole regions are generally flatter than high-index regions and have a greater influence on ion trajectories.[43] Figure 2d is not the actual tip shape; as noted above, the nanowire cross section is triangular due to anisotropic growth rates on different crystal planes.

For comparison, Figure 2e shows faceting similar to what was observed by Jindal et al. during selected area growth of GaN and was explained in terms of the growth velocities for distinct facets.[36] Similarly, under APT analysis conditions, anisotropic *evaporation* results in faceting that reflects the relative stability of various facets. The actual tip shape is therefore likely intermediate to Figure 2d and e.

Variations in the hit density of particular species (Figure 3) can provide additional insights into the influence of the crystal structure on ion evaporation and the facets that are present during APT analysis. The Ga⁺ and N₂⁺ hit densities show the same symmetries and trends, with fewer ions detected in a band running through the middle of the map and fewer ions detected toward the Ga-polar surface (toward the top of the figure). The band of low hit density is due to evaporation at locally higher electric fields; the edges of atomic terraces cause local enhancements in the
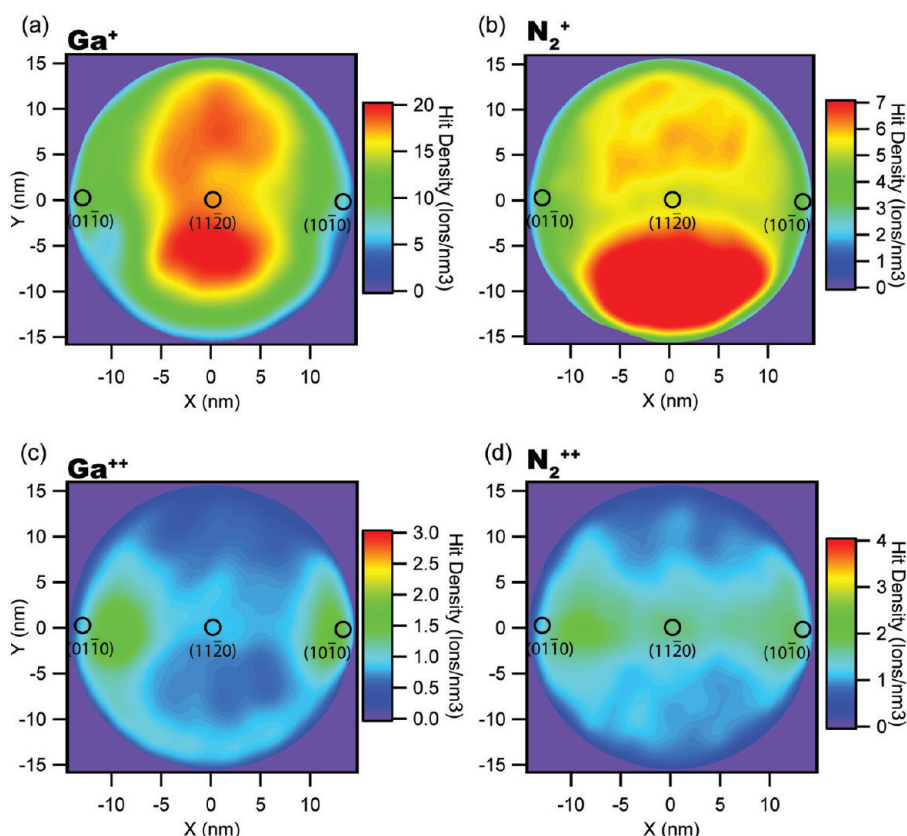
Figure 3. 2-D hit density profiles for (a) Ga^+ (b) N_2^+ (c) Ga^{++}, and (d) N_2^{++}. Regions of high curvature are associated with a relative increase in doubly ionized species.

electric field at the edges of low-index planes, such as the central *a*-plane, leading to increased evaporation of doubly charged ions as shown in Figure 3c,d. The ratio of doubly charged to singly charged ions corroborates the identification of high-field regions associated with the crystallographic poles. The variation in hit density with facet polarity is discussed further below, along with detailed analyses of other factors influencing the density of detected ions in this materials system, following an examination of the stoichiometry.

The facet polarity strongly influences the relative evaporation rates of Ga and N, leading to apparent local variations in stoichiometry even when the composite mass spectrum is stoichiometric (Figure 4). For the APT analysis that generated the 2-D concentration profile in Figure 4, the evaporation conditions were tuned to achieve stoichiometric detection of the *total* number of Ga and N ions. However, upon inspection of the 2-D profile, it becomes clear that stoichiometric detection was only occurring near the N-polar surface of the nanowire (bottom of Figure 4a). The nonpolar and Ga-polar surfaces exhibit a N deficit. The total numbers of Ga and N atoms were detected in the expected stoichiometric ratio because a higher proportion of atoms was being collected from regions near the N-polar surface (as shown in Figure 3a,b) where the apparent stoichiometry is closest to the actual stoichiometry. As the polar

c-axis is also normal to the *m*-axis, a similar trend would be observed in nanowires grown or analyzed along the nonpolar *m*-axis. The observed deviations in stoichiometry are dominated by the preferential loss of nitrogen-containing ions. An ion is "lost" when its evaporation is uncorrelated with the laser pulse, which is the case for evaporation between laser pulses, or during a multiple hit event, which is defined as two or more ions evaporating from the specimen following a single laser pulse.[44] Multiple hits can occur, for example, when an additional ion evaporates while the nanowire tip is cooling following the laser pulse, leading to thermal tails on the mass spectrum peaks (inset, Figure 1c). The ion appears at a higher than expected m/n value because of the extra time that elapses between the laser pulse incidence and the actual evaporation event.

In general, more N_2 than Ga evaporates in multiple hit events, so a higher fraction of N ions is not detected. This tendency is illustrated in Table 1. N_2 loss is especially pronounced at nonpolar and Ga-polar surfaces (Figure 4) due to the variations of bonding coordination at these surfaces. To explain the absence of N^+ ions and the dominance of N_2^+ ions in the spectra, we propose that the rate-limiting step for the evaporation of N on nonpolar and Ga-polar regions is surface diffusion of N to form N_2. Migration of N is the most plausible formation mechanism for N_2; the
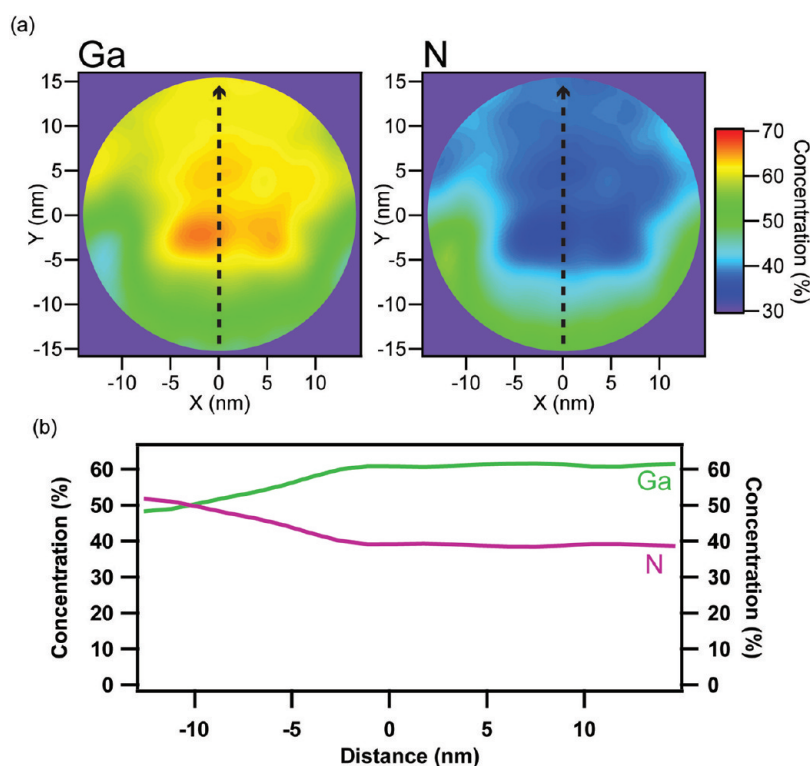
Figure 4. (a) 2-D and (b) 1-D concentration profiles depicting stoichiometric evaporation occurring near the N-polar surface (bottom) with decreased N and increased Ga detection near the nonpolar (center) and Ga-polar (top) surfaces. These profiles were generated from APT data that exhibited overall stoichiometric evaporation. Distance on the 1-D profile corresponds to distance along the dashed arrows in (a).

TABLE 1. Number of Single and Multiple Hits Measured for the Majority Species during APT Analysis

	Ga$^+$	Ga^{2+}	N$_2^+$	N$_2^{2+}$
% single	83	54	61	32
% multiple	17	46	39	68

wurtzite crystal has no N—N bonds, and it is unlikely that two N atoms would combine under vacuum while traveling to the detector. Formation of group V clusters during APT analysis has been previously observed in III—As and III—P materials and attributed to surface migration.[20−23,25] While higher-order clusters of As and P were observed (up to 7 atoms),[23] higher-order clusters of N are not observed because N$_2$ is stable and likely has a negligible barrier to evaporation.[45,46] The hypothesis of diffusion-limited evaporation, with the barrier to N diffusion lower than the barrier to N$^+$ evaporation but higher than the N$_2$ desorption barrier, is consistent with calculations: the barrier for the diffusion of a N adatom on a Ga-polar surface is 0.66 eV,[47] whereas the estimated Ga—N bond energy is 4.2 eV.[48,49]

Despite the distinct evaporation behaviors of the group III and group V elements, analysis conditions could be tuned so that the total amounts of Ga and N atoms detected are equal. The adjustable experimental parameters include the specimen temperature, laser pulse repetition rate, laser pulse energy, and applied dc
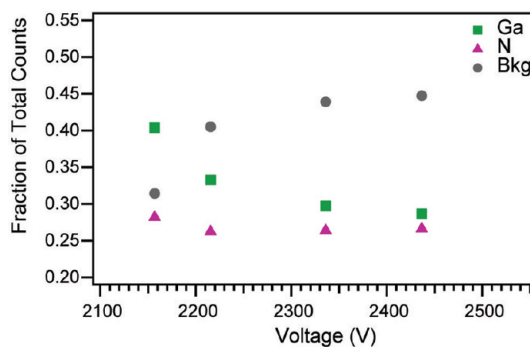

Figure 5. Fraction of Ga, N, and background counts for different voltages. Laser pulse energy, repetition rate, and specimen temperature are held constant. Background counts are defined as counts not originating from the Ga or N peaks.

voltage. Using the lowest specimen temperature (∼37 K) improved Ga and N detection by increasing the cooling rate, which reduces the cooling-limited peak width (see Figure 1c inset) and the amount of uncorrelated evaporation. Increasing the laser pulse repetition rate slightly improved the spectrum quality by reducing the number of uncorrelated evaporation events between pulses. At low laser pulse energies (0.014−0.532 pJ), the detection efficiency was insensitive to pulse energy.

The dc voltage had the most significant influence on Ga and N detection. The N/Ga ratio approached the stoichiometric value when the applied dc voltage was

increased by raising the target evaporation rate during APT analysis. However, this apparent improvement was actually due to a decrease in Ga detection rather than an increase in N detection, as illustrated in Figure 5. Ga depletion at high applied dc voltages has been previously observed in GaAs[19] and was attributed to the fact that the evaporation field of Ga (15 V/nm) is far lower than that of As (42 V/nm).[19,23,39,50] These evaporation field values have been tabulated and described in detail elsewhere.[50] The evaporation fields used in this discussion have been calculated for elemental species and likely differ for atoms present in a compound, but the values inform a qualitative discussion of evaporation behaviors. Both As and N are group V elements that display qualitatively similar evaporation with a proclivity for thermally assisted surface migration and evaporation as higher-order molecular ions,[22,23,25] so it is reasonable to conclude that the Ga deficit increases with increasing dc voltage because it has a lower evaporation field than N. Once dc field evaporation of Ga becomes significant, the noise level in the mass spectrum increases because these events are not correlated with the laser pulse. If the dc voltage is increased even further, both Ga and N are expected to dc field evaporate, leading to a deficit in both species and a further increase in the background of the mass spectrum, which was also observed to occur for Ga and As in GaAs.[19]

DISCUSSION OF IMPLICATIONS FOR ANALYSIS OF III−N HETEROSTRUCTURES

The results reported above raise the important question of whether pulsed laser APT is a reliable technique for the analysis of III−N heterostructures. We conclude that reliable analysis is possible provided the distinct evaporation behaviors of the constituent species are accounted for. Due to the difference in the evaporation fields of Ga and N and the polarity-induced deviations in the local evaporation of Ga and N

atoms, empirically adjusting experimental conditions to obtain global detection of Ga and N in the correct stoichiometric ratio may not be appropriate. In fact, the experimental conditions that yield apparent stoichiometric evaporation increase the background of the mass spectrum associated with uncorrelated evaporation, making it difficult to study dilute species such as dopants. Improvements in the stoichiometry (i.e., N detection) may result from operation at higher pulse frequencies and better focused laser excitation through improvements in in situ vacuum optics. More focused laser pulses decrease the time at which the tip temperature is sufficient to produce diffusion by generating larger thermal gradients and enabling the use of lower pulse energies.

In order to best analyze dopants or other group III elements in III−N ternary alloys that may be present in low concentrations, experimental conditions should be optimized to provide high mass resolution and low background levels. On the basis of the observed Ga deficit caused by dc field evaporation at high applied voltages, it is probable that the signal-to-noise of the mass spectrum will be highest at low applied voltages. Maximizing the signal-to-noise should result in the optimized detection of Ga and other species incorporated substitutionally on Ga sites, such as Mg dopants in p-GaN and In or Al in $In_xGa_{1-x}N$ or $Al_xGa_{1-x}N$, respectively. The evaporation fields of Mg (21 V/nm), In (12 V/nm), and Al (19 V/nm) are similar to that of Ga (15 V/nm).[39,50] Because these species occupy Ga lattice sites in the GaN matrix and have comparable calculated evaporation fields, it is likely that their evaporation behaviors will be similar to that of Ga. The ability to detect low concentrations of p-dopants and group III elements in III−GaN alloys will enable APT to analyze doping efficiency and interface abruptness, which is particularly useful for the advancement of GaN-based heterostructures.

MATERIALS AND METHODS

a-Axis Mg-doped nanowires were grown via MOCVD using Ni catalysts on *r*-plane sapphire as described previously.[31,51] The nanowires were grown using a trimethylgallium precursor with a flow rate of 1.41 mmol/min and doped using bis-(cyclopentadienyl)magnesium with a flow rate of 4.30×10^{-3} mmol/min. Nanowires were mechanically transferred from the growth substrate to a half TEM grid using a manual micromanipulator and an optical microscope. A nanomanipulator in a SEM was then used to select nanowires greater than 8 μm in length and less than 100 nm diameter and transfer these nanowires from the grid to tungsten microtips. Finally, electron-beam-induced deposition of platinum was used to form a moderately conducting and mechanically stable joint.[29] A local electrode atom probe 4000× Si was used to perform APT analysis. The following conditions were used during APT analysis: laser pulse energy of 0.014−0.532 pJ, laser pulse repetition rate of 250, 500, or 750 kHz, base temperature of 37−84 K, and applied dc voltage of 2123−2786 V. Run conditions were chosen such that the mass spectrum was relatively insensitive

to variations in the laser power. The sensitivity of stoichiometry to the dc voltage was previously discussed.

Conflict of Interest: The authors declare no competing financial interest.

and discussions regarding multiple hit analysis. Sandia National Laboratories is a multiprogram laboratory managed and operated by Sandia Corporation, a wholly owned subsidiary of Lockheed Martin Corporation, for the U.S. Department of Energy's National Nuclear Security Administration under contract DE-AC04-94AL85000.

REFERENCES AND NOTES

1. Nakamura, S. *The Blue Laser Diode: The Complete Story*; Springer-Verlag: Berlin, 2000.

2. Shen, H.; Wraback, M.; Zhong, H.; Tyagi, A.; DenBaars, S. P.; Nakamura, S.; Speck, J. S. Unambiguous Evidence of the Existence of Polarization Field Crossover in a Semipolar InGaN/GaN Single Quantum Well. *Appl. Phys. Lett.* **2009**, *95*, 033503.

3. Prosa, T. J.; Clifton, P. H.; Zhong, H.; Tyagi, A.; Shivaraman, R.; DenBaars, S. P.; Nakamura, S.; Speck, J. S. Atom Probe Analysis of Interfacial Abruptness and Clustering Within a Single In[x]Ga[1−x]N Quantum Well Device on Semipolar (10-1-1) GaN Substrate. *Appl. Phys. Lett.* **2011**, *98*, 191903.

4. Polyakov, A. Y.; Smirnov, N. B.; Govorkov, A. V.; Amano, H.; Pearton, S. J.; Lee, I. H.; Sun, Q.; Han, J.; Karpov, S. Y. Role of Nonradiative Recombination Centers and Extended Defects in Nonpolar GaN on Light Emission Efficiency. *Appl. Phys. Lett.* **2011**, *98*, 072104.

5. Watanabe, S.; Yamada, N.; Nagashima, M.; Ueki, Y.; Sasaki, C.; Yamada, Y.; Taguchi, T.; Tadatomo, K.; Okagawa, H.; Kudo, H. Internal Quantum Efficiency of Highly-Efficient In[x]Ga[1−x]N-Based Near-Ultraviolet Light-Emitting Diodes. *Appl. Phys. Lett.* **2003**, *83*, 4906–4908.

6. Galtrey, M. J.; Oliver, R. A.; Kappers, M. J.; McAleese, C.; Zhu, D.; Humphreys, C. J.; Clifton, P. H.; Larsen, D.; Cerezo, A. Atom Probe Reveals the Structure of In[x]Ga[1−x]N Based Quantum Wells in Three Dimensions. *Phys. Status Solidi B* **2008**, *245*, 861–867.

7. Oliver, R. A.; Bennett, S. E.; Zhu, T.; Beesley, D. J.; Kappers, M. J.; Saxey, D. W.; Cerezo, A.; Humphreys, C. J. Microstructural Origins of Localization in InGaN Quantum Wells. *J. Phys. D Appl. Phys.* **2010**, *43*, 354003.

8. Qian, F.; Li, Y.; Gradecak, S.; Wang, D.; Barrelet, C. J.; Lieber, C. M. Gallium Nitride-Based Nanowire Radial Heterostructures for Nanophotonics. *Nano Lett.* **2004**, *4*, 1975–1979.

9. Qian, F.; Gradecak, S.; Li, Y.; Wen, C.; Lieber, C. Core/Multishell Nanowire Heterostructures as Multicolor, High-Efficiency Light-Emitting Diodes. *Nano Lett.* **2005**, *5*, 2287–2291.

10. Ke, M.-Y.; Wang, C. Y.; Chen, L. Y.; Chen, H. H.; Chiang, H. L.; Cheng, Y. W.; Hsieh, M. Y.; Chen, C. P.; Huang, J. Application of Nanosphere Lithography to LED Surface Texturing and to the Fabrication of Nanorod LED arrays. *IEEE J. Sel. Top. Quant.* **2009**, *15*, 1242–1249.

11. Chiu, C. H.; Lu, T. C.; Huang, H. W.; Lai, C. F.; Kao, C. C.; Chu, J. T.; Yu, C. C.; Kuo, H. C.; Wang, S. C.; Lin, C. F.; *et al.* Fabrication of InGaN/GaN Nanorod Light-Emitting Diodes with Self-Assembled Ni Metal Islands. *Nanotechnology* **2007**, *18*, 445201.

12. Seidman, D. N. Three-Dimensional Atom-Probe Tomography: Advances and Applications. *Ann. Rev. Mater. Res.* **2007**, *37*, 127–158.

13. Seidman, D. N.; Stiller, K. An Atom Probe Tomography Primer. *MRS Bull.* **2009**, *34*, 717–724.

14. Perea, D. E.; Wijaya, E.; Lensch-Falk, J. L.; Hemesath, E. R.; Lauhon, L. J. Tomographic Analysis of Dilute Impurities in Semiconductor Nanostructures. *J. Solid State Chem.* **2008**, *181*, 1642–1649.

15. Perea, D. E.; Hemesath, E. R.; Schwalbach, E. J.; Lensch-Falk, J. L.; Voorhees, P. W.; Lauhon, L. J. Direct Measurement of Dopant Distribution in an Individual Vapour-Liquid-Solid Nanowire. *Nat. Nanotechnol.* **2009**, *4*, 315–319.

16. Schlitz, R. A.; Perea, D. E.; Lensch-Falk, J. L.; Hemesath, E. R.; Lauhon, L. J. Correlating Dopant Distributions and Electrical Properties of Boron-Doped Silicon Nanowires. *Appl. Phys. Lett.* **2009**, *95*, 162101.

17. Sakurai, T.; Hashizume, T.; Jimbo, A.; Sakata, T. An Atom-Probe Study of III-V Compound Semiconductors. *J. Phys. Colloques* **1984**, *45*, 453–458.

18. Cerezo, A.; Grovenor, C. R. M.; Smith, G. D. W. Pulsed Laser Atom Probe Analysis of GaAs and InAs. *Appl. Phys. Lett.* **1985**, *46*, 567–569.

19. Hashizume, T.; Hasegawa, Y.; Kobayashi, A.; Sakurai, T. Atom-Probe Investigation of III−V Semiconductors: Comparison of Voltage-Pulse and Laser-Pulse Modes. *Rev. Sci. Instrum.* **1986**, *57*, 1378–1380.

20. Yamamoto, M.; Seidman, D. N.; Nakamura, S. A Study of the Composition of the {111} Planes of GaP on an Atomic Scale. *Surf. Sci.* **1982**, *118*, 555–571.

21. Gaussmann, A.; Drachsel, W.; Block, J. H. Kinetics of Field Evaporation During Hydride Formation on GaP Surfaces: a FIM and Atom-Probe Study. *Langmuir* **1992**, *8*, 125–129.

22. Gorman, B. P.; Norman, A. G.; Yan, Y. Atom Probe Analysis of III-V and Si-Based Semiconductor Photovoltaic Structures. *Microsc. Microanal.* **2007**, *13*, 493–502.

23. Liddle, J. A.; Norman, A.; Cerezo, A.; Grovenor, C. R. M. Pulsed Laser Atom Probe Analysis of Ternary and Quaternary III-V Epitaxial Layers. *J. Phys. Colloques* **1988**, *49*, 509–514.

24. Mackenzie, R. A. D.; Liddle, J. A.; Grovenor, C. R. M. Compositional Homogeneity of Metalorganic Chemical Vapor Deposition Grown III-V Compound Semiconductor Epilayers. *J. Appl. Phys.* **1991**, *69*, 250–256.

25. Gorman, B. P.; Guthrey, H.; Norman, A.; Al-Jassim, M.; Lawrence, D.; Prosa, T. J. Atomic Scale Characterization of Compound Semiconductors using Atom Probe Tomography. In *IEEE Photovoltaic Specialists Conference*, Seattle, WA, **2011**; pp 1−3.

26. Perea, D. E.; Lensch, J. L.; May, S. J.; Wessels, B. W.; Lauhon, L. J. Composition Analysis of Single Semiconductor Nanowires using Pulsed-Laser Atom Probe Tomography. *Appl. Phys. A: Mater. Sci. Processes* **2006**, *85*, 271–275.

27. Galtrey, M. J.; Oliver, R. A.; Kappers, M. J.; Humphreys, C. J.; Stokes, D. J.; Clifton, P. H.; Cerezo, A. Three-Dimensional Atom Probe Studies of an In[x]Ga[1−x]N/GaN Multiple Quantum Well Structure: Assessment of Possible Indium Clustering. *Appl. Phys. Lett.* **2007**, *90*, 061903.

28. Bennett, S. E.; Clifton, P. H.; Ulfig, R. M.; Kappers, M. J.; Barnard, J. S.; Humphreys, C. J.; Oliver, R. A. Mg Dopant Distribution in an AlGaN/GaN p-type Superlattice Assessed Using Atom Probe Tomography. *TEM and SIMS. J. Phys. Conf. Ser.* **2010**, *209*, 012014.

29. Agrawal, R.; Bernal, R. A.; Isheim, D.; Espinosa, H. D. Characterizing Atomic Composition and Dopant Distribution in Wide Band Gap Semiconductor Nanowires Using Laser-Assisted Atom Probe Tomography. *J. Phys. Chem. C* **2011**, *115*, 17688–17694.

30. Coursey, J. S.; Schwab, D. J.; Tsai, J. J.; Dragoset, R. A. Atomic Weights and Isotopic Compositions (version 3.0). http://physics.nist.gov/Comp (accessed October 8, 2011).

31. Wang, G. T.; Talin, A. A.; Werder, D. J.; Creighton, J. R.; Lai, E.; Anderson, R. J.; Arslan, I. Highly Aligned, Template-Free Growth and Characterization of Vertical GaN Nanowires on Sapphire by Metal-Organic Chemical Vapour Deposition. *Nanotechnology* **2006**, *17*, 5773–5780.

32. Li, Q.; Creighton, J. R.; Wang, G. T. The Role of Collisions in the Aligned Growth of Vertical Nanowires. *J. Cryst. Growth* **2008**, *310*, 3706–3709.

33. Mastro, M. A.; Simpkins, B.; Wang, G. T.; Hite, J.; Eddy, C. R., Jr.; Kim, H. Y.; Ahn, J.; Kim, J. Polarization Fields in III-Nitride Nanowire Devices. *Nanotechnology* **2010**, *21*, 145205.

34. Li, Q.; Wang, G. T. Strain Influenced Indium Composition Distribution in GaN/InGaN Core-Shell Nanowires. *Appl. Phys. Lett.* **2010**, *97*, 181107.

35. Qian, F.; Li, Y.; Gradecak, S.; Park, H. G.; Dong, Y.; Ding, Y.; Wang, Z. L.; Lieber, C. M. Multi-Quantum-Well Nanowire Heterostructures for Wavelength-Controlled Lasers. *Nat. Mater.* **2008**, *7*, 701–706.

36. Jindal, V.; Shahedipour-Sandvik, F. Theoretical Prediction of GaN Nanostructure Equilibrium and Nonequilibrium Shapes. *J. Appl. Phys.* **2009**, *106*, 083115.

37. Northrup, J. E.; Neugebauer, J. Strong Affinity of Hydrogen for the GaN(000−1) Surface: Implications for Molecular Beam Epitaxy and Metalorganic Chemical Vapor Deposition. *Appl. Phys. Lett.* **2004**, *85*, 3429–3431.

38. Ng, H. M.; Weimann, N. G.; Chowdhury, A. GaN Nanotip Pyramids Formed by Anisotropic Etching. *J. Appl. Phys.* **2003**, *94*, 650–653.

39. Miller, M. K. *Atom Probe Tomography: Analysis at the Atomic Level*; Kluwer Academic/Plenum Publishers: New York, 2000.

40. Marquis, E. A.; Vurpillot, F. Chromatic Aberrations in the Field Evaporation Behavior of Small Precipitates. *Microsc. Microanal.* **2008**, *14*, 561–570.

41. Vurpillot, F.; Bostel, A.; Blavette, D. The Shape of Field Emitters and the Ion Trajectories in Three-Dimensional Atom Probes. *J. Microsc.* **1999**, *196*, 332–336.

42. Gault, B.; Moody, M. P.; de Geuser, F.; Tsafnat, G.; La Fontaine, A.; Stephenson, L. T.; Haley, D.; Ringer, S. P. Advances in the Calibration of Atom Probe Tomographic Reconstruction. *J. Appl. Phys.* **2009**, *105*, 034913.

43. De Geuser, F.; Gault, B.; Bostel, A.; Vurpillot, F. Correlated Field Evaporation as Seen by Atom Probe Tomography. *Surf. Sci.* **2007**, *601*, 536–543.

44. Saxey, D. W. Correlated Ion Analysis and the Interpretation of Atom Probe Mass Spectra. *Ultramicroscopy* **2011**, *111*, 473–479.

45. Grzegory, I.; Jun, J.; Bockowski, M.; Krukowski, S.; Wroblewski, M.; Lucznik, B.; Porowski, S. III−V Nitrides—Thermodynamics and Crystal Growth at High N2 Pressure. *J. Phys. Chem. Solids* **1995**, *56*, 639–647.

46. Fernández-Garrido, S.; Koblmüller, G.; Calleja, E.; Speck, J. S. In situ GaN Decomposition Analysis by Quadrupole Mass Spectrometry and Reflection High-Energy Electron Diffraction. *J. Appl. Phys.* **2008**, *104*, 033541.

47. Jindal, V.; Shahedipour-Sandvik, F. Computational and Experimental Studies on the Growth of Nonpolar Surfaces of Gallium Nitride. *J. Appl. Phys.* **2010**, *107*, 054907.

48. Koleske, D. D.; Wickenden, A. E.; Henry, R. L.; DeSisto, W. J.; Gorman, R. J. Growth Model for GaN with Comparison to Structural, Optical, and Electrical Properties. *J. Appl. Phys.* **1998**, *84*, 1998–2010.

49. Seki, Y.; H., W.; Matsui, J. Impurity Effect on Grown-In Dislocation Density of InP and GaAs Crystals. *J. Appl. Phys.* **1978**, *49*, 822–828.

50. Tsong, T. T. Field Ion Image Formation. *Surf. Sci.* **1978**, *70*, 211–233.

51. Li, Q.; Wang, G. T. Improvement in Aligned GaN Nanowire Growth Using Submonolayer Ni Catalyst Films. *Appl. Phys. Lett.* **2008**, *93*, 043119.